1. Introduction

Perovskites (ABO_3) are a prominent topic of research in materials science (high-T_c-electric conductor [1, 2], ferroelectric [3, 4] or high k dielectric [5], or magnetoresistance [6] material). Doping of these perovskites with multivalent cations on the A- and B- sites can lead to the simultaneous occurrence of ionic and electronic conductivities. For example, the partial substitution of Sr and Co for La and Fe in the A- and B- sites of $LaFeO_3$ can result in a mixed conductor because oxygen vacancy defects (δ) are formed at the elevated temperature [7]. In recent years, such perovskite-type membranes with mixed ionic and electronic conductivities are of interest not only for a simple oxygen separation [8], but also for their potential use in the membrane reactor for the conversion of hydrocarbons, such as the partial oxidation of methane to syngas ($CO + H_2$) [9-12] and the oxidative dehydrogenation of alkanes to alkenes [13-17].

Fig. 1 illustrates the oxygen permeation through a dense perovskite membrane driven by an oxygen partial pressure gradient across it. The oxygen permeation involves three steps. At first, the oxygen molecules become reduced to oxygen ions at the membrane surface exposed to the high oxygen partial pressure (air side). Then, the oxygen ions diffuse in the bulk in the form of the oxygen vacancy and the electrons diffuse in opposite direction through the bulk of the membrane. Finally, the oxygen ions recombine to form the oxygen molecules at the membrane surface exposed to the low oxygen partial pressure (sweep side). The oxygen permeation flux through the perovskite membranes is

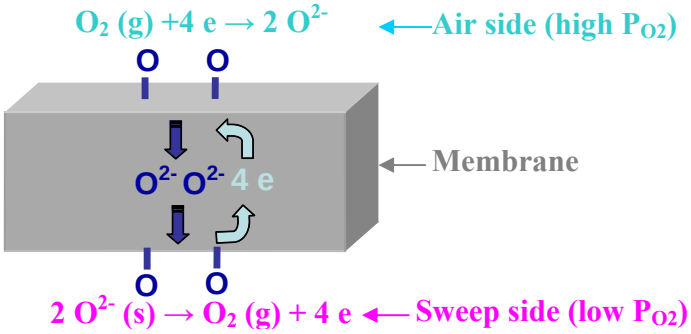

Fig. 1 Mechanism of the oxygen transport through dense perovskite membranes.

essentially controlled by two factors, by (i) the rate of the oxygen vacancy diffusion within the membrane and by (ii) the interfacial oxygen exchange on either side of the membrane. The oxygen permeation flux can be increased by reducing the thickness of the membrane, until its thickness becomes less than a characteristic value, L_c, at which the oxygen transport is equally limited by both the surface exchange kinetics and the bulk diffusion. Below L_c, a further decrease of the membrane thickness does not result in a remarkable increase of the oxygen permeation flux. Therefore, it is very important to understand the transport mechanism of oxygen through the perovskite membranes. ^{18}O – ^{16}O isotopic exchange techniques were usually used to measure the oxygen vacancy diffusion coefficient and the surface exchange coefficient, from which the limiting step of the oxygen transport can be determined.

In this paper, we deduced the limiting step of the oxygen transport in the perovskite membranes and determined the oxygen vacancy diffusion coefficient (D_v) from oxygen permeation measurements as a function of the oxygen pressure gradient and the membrane thickness. The $Ba_{0.5}Sr_{0.5}Co_{0.8}Fe_{0.2}O_{3-\delta}$ (BSCF) was chosen for this study

because it is an excellent perovskite membrane which was widely studied for oxygen separation [8, 18] and as a membrane reactor for the partial oxidation of methane to syngas [10, 12], and for the selective oxidation of light hydrocarbons [14, 16, 17].

2. Experimental

The BSCF oxide powder was synthesized by a combined citrate and EDTA complexing method [18]. The oxygen content in the BSCF at indicated temperatures can be determined by a thermogravimetric analyzer (TA Instruments). The membrane tube was prepared by the plastic extrusion method [19]. The sintered membrane tube has an outer diameter of about 8.0 mm, an inner diameter of about 5.0 mm. The densities of the sintered tubular membranes were measured by the Archimedes method with ethanol. Only those membranes that had the relative density higher than 90% were used for the permeation study. A shell-and-tube permeation cell (permeator) was used for oxygen permeation which was described in reference [8]. The membrane tube, which was connected with two quartz tubes (Φ = 17 mm) sealed with groove at their ends, served as the tube side. Another quartz tube (Φ = 29 mm) served as the shell side of the permeator. A tubular furnace was used to heat the permeator. The temperature was controlled by a microprocessor temperature controller (Model Al-708, Xiamen Yuguang Electronics Technology Research Institute) within $\pm$1 K of the set points and monitored by a K-type thermocouple encased near the tube. The inlet gas flow rates were controlled by mass flow controllers (model D07-7A/ZM, Beijing Jianzhong Machine Factory, China). High

purity helium (>99.999%) was used as a sweep gas on the tube side of the permeator. GC (HP6890) equipped with a 3m 5A molecular sieve column for the separation of O_2 and N_2 was connected to the exit of the tube side to determine the O_2 concentration.

The oxygen permeation measurement of the BSCF membrane tube was studied for different combinations of temperatures and oxygen partial pressures on the shell side (P_1) and on the tube side (P_2). The total flow rate of a mixture of O_2 and N_2 on the shell side was 300ml/min and different oxygen partial pressures (P_1) on the shell side can be obtained by adjusting the ratio of N_2 and O_2. The helium flow rate on the tube side was 60ml/min. The oxygen partial pressure (P_2) on the tube side can be calculated by using the formula: $P_2=C_{O2}\times P_0$ (P_0 is 1 atm oxygen pressure). So the oxygen partial pressure (P_2) is equal to the oxygen concentration (C_{O2}) which can be measured with the GC (HP6890) and the data were acquired under conditions where P_1 was varied step by step while the temperature was kept constant and vice versa where the temperature was varied in steps while P_1 was kept constant.

3. Result and discussion

Fig. 2 shows the oxygen content in the BSCF oxide at different temperatures. The oxygen content was determined by thermogravimetric analysis. First, the BSCF oxide was pretreated in air with a flow rate of 60 ml/min at 950 ^oC for 2h to remove the traces of water. After the temperature was decreased to room temperature, a mixture of 5% H_2 and

95% Ar was used to reduce the sample by increasing the temperature to 900 ^{o}C at a heating rate of 10 ^{o}C/min. The sample was held at 900 ^{o}C for 3h to ensure its complete reduction. During the hydrogen reduction, the BSCF underwent the following decomposition:

$$Ba_{0.5}Sr_{0.5}Co_{0.8}Fe_{0.2}O_{3-\delta} \rightarrow 0.5SrO + 0.5BaO + 0.8Co + 0.2Fe + \frac{2-\delta}{2}O_2(gas)$$

Based on the above equation and the weight loss（13.27%), the oxygen content in the BSCF was calculated to be 3-δ = 2.79 at the room temperature with δ as the oxygen vacancy defects called the oxygen non-stoichiometry.

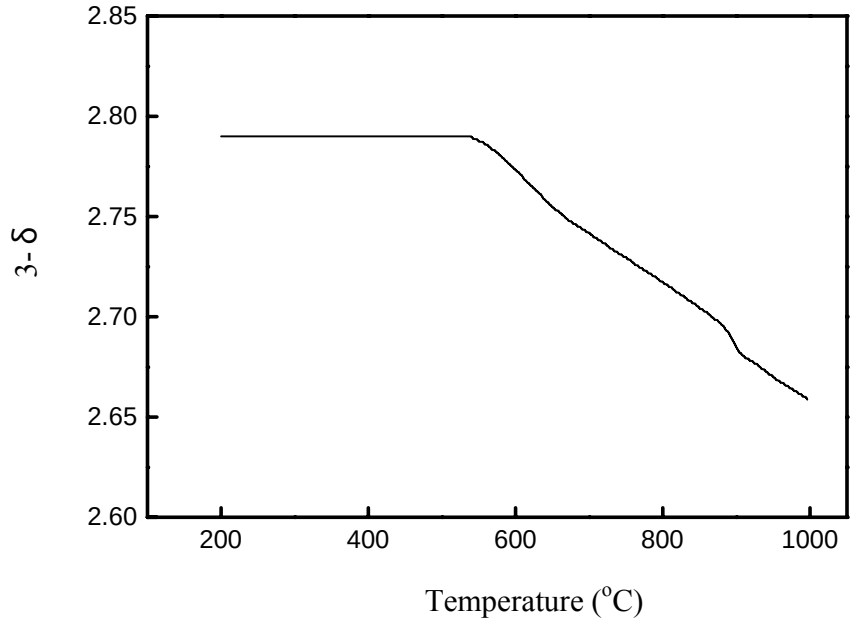

Fig. 2 Development of oxygen cacancy defects (δ) as a function of temperature as derived from thermogravimetric data for the BSCF oxide in air.

The oxygen content in the BSCF at other temperatures can be determined by a thermogravimetric analyzer. Measurements were carried out up to 1000 ^{o}C at a heating

rate of 10 °C/min in air with a flow rate of 60 ml/min. The oxygen content at different temperatures can be calculated from the TG curve. As shown in Fig. 2, the oxygen content decreases with increasing temperature.

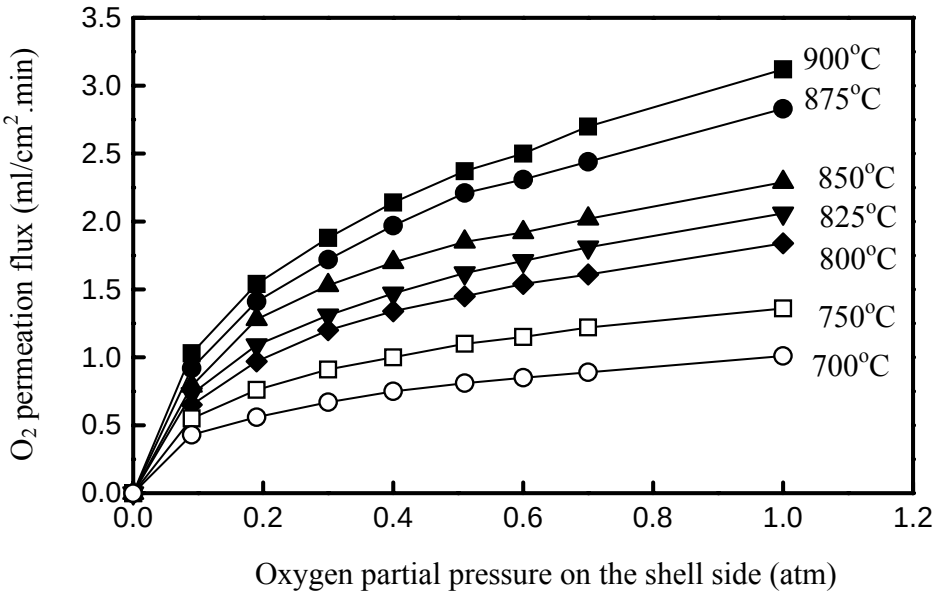

Fig. 3 Oxygen permeation flux through the BSCF membrane tube as a function of the oxygen partial pressure on the shell side.
Flow rates: a mixture of O_2 and N_2 = 300 ml/min, He = 60 ml/min, P_1 varied from 0.09 atm to 1atm; P_2 varied from 0.0093 atm to 0.1147 atm. $Ø_2$=7.96 mm, $Ø_1$=4.56 mm, L=17.68 mm, S=2.531 cm^2.

Fig. 3 gives the oxygen permeation flux through the BSCF membrane tube as a function of the oxygen partial pressures on the shell side at temperatures from 700 °C to 900 °C. As shown in Fig. 3, the oxygen permeation flux increases with increasing oxygen partial pressure on the shell side. The oxygen permeation flux reaches 3.0 ml/cm^2.min at 900 °C under the oxygen partial pressure of 1.0 atm on the shell side. This result indicates that the sufficient oxygen permeation flux demanded for an industrial application can be

achieved by increasing the air pressure on the shell side. The oxygen permeation flux increases with increasing temperatures, which can be attributed to the increase of the oxygen diffusion with rising temperatures.

As mentioned in the introduction, it is important to understand the limiting step of the oxygen transport through the perovskite membrane. Therefore, the surface exchange fluxes model reported by S. Kim [20, 21] was used to interpret the experimental data for the BSCF membrane tube. The exchange flux i_i at the perovskite membrane – gas interfaces at the inlet and outlet sides is given by [20]:

$$i_i = k_{i,0} c_i (e^{n\mu_g / RT} - e^{2n\mu / RT}) \quad (1)$$

where $k_{i,o}$ is the surface exchange coefficient, C_i is the density of oxygen ions, n is the reaction order at the interfaces, μ is the chemical potential of the oxygen ions at the two interfaces, and μ_g is the chemical potential of the gas

$$\mu_g = RT \ln(p / p_0) \quad (2)$$

where P is the gas pressure and the subscript 0 indicates the standard pressure of 1.0 atm. At the interfaces, the following reaction occurs:

$$\frac{1}{2} O_2 + V_O^{\bullet\bullet} \rightleftarrows O^{2-} + 2h^{\bullet} \quad (3)$$

with $V_O^{\bullet\bullet}$ and $h^{\bullet}$ as the oxygen vacancy and the electron hole, respectively.

Thus the reaction order, n at the interfaces is n = ½. The exchange oxygen fluxes i_1 and i_2 at the perovskite membrane – gas interfaces at the inlet and outlet sides are given by:

$$i_1 = k_{i,0} c_i (e^{\mu_{1g} / 2RT} - e^{\mu_1 / RT}) \quad (4)$$

$$i_2 = k_{i,0} c_i (e^{\mu_2 / RT} - e^{\mu_{2g} / 2RT}) \quad (5)$$

On the other hand, the flux density is determined by the charge, conductivity and the gradient of the electrochemical potential. Therefore, the oxygen ionic flux i_i can be also described by [22]:

$$i_i = -\frac{\sigma_i}{2F}\frac{d\mu}{d\phi} \quad (6)$$

where Ø is the diameter of the membrane tube, σ_i is the oxygen ion conductivity.

The oxygen ion conductitivity is also determined by the oxygen ion diffusion coefficient D_i and the oxygen ion concentration C_i in the perovskites [22]

$$\sigma_i = \frac{D_i}{RT} 4F^2 C_i \quad (7)$$

By combining Eqs. (6) and (7) we get the oxygen permeation flux j_{O_2},

$$j_{O_2} = \frac{i_i}{2F} = -\frac{\sigma_i}{4F^2}\frac{d\mu}{d\phi} = -\frac{D_i C_i}{RT}\frac{d\mu}{d\phi} \quad (8)$$

The normalized oxygen permeation flux j_{O_2} can be expressed as:

$$j_{O_2} = F \big/ \pi\phi L \quad (9)$$

where, L is the length of the membrane tube, $\pi\phi L$ is the membrane surface, F is the total oxygen flux through the membrane.

By combining Eqs. (8) and (9) we can get:

$$-\frac{D_i C_i}{RT}\frac{d\mu}{d\phi} = F \big/ \pi\phi L \quad (10)$$

Continuity of ion flux requires that the surface exchange fluxes and the oxygen permeation flux j_{O_2} at the two interfaces match:

$$F \Big/ \pi\phi_1 L = k_{i,0} c_i (e^{\mu_{1g}/2RT} - e^{\mu_1/RT}) \tag{11}$$

$$F \Big/ \pi\phi_2 L = k_{i,0} c_i (e^{\mu_2/RT} - e^{\mu_{2g}/2RT}) \tag{12}$$

Integrating of Eq. (10) yields:

$$\mu_2 - \mu_1 = \frac{RTF}{\pi c_i D_i L} \ln(\phi_2 / \phi_1) \tag{13}$$

where ϕ_1 and ϕ_2 are the inner and outer diameters of the membrane tube

The following relation can be obtained by eliminating μ_1 and μ_2 in Eqs. (11) – (13)

$$\frac{F}{\pi c_i D_i L} \ln(\phi_2 / \phi_1) = \ln\left(\frac{\sqrt{P_1 / P_0} - F / \pi\phi_2 L C_i k_{i,0}}{\sqrt{P_2 / P_0} + F / \pi\phi_1 L C_i k_{i,0}} \right) \tag{14}$$

If the oxygen transport is limited by the surface exchange, $\mu_1 \to \mu_2$, so Eq. (14) reduces to:

$$F = \frac{\pi\phi_1\phi_2 L c_i k_{i,0}}{\phi_1 + \phi_2} \left(\sqrt{P_1 / P_0} - \sqrt{P_2 - P_0} \right) \tag{15}$$

On the other hand, if the oxygen transport is limited by the bulk diffusion, $\mu_1 \to \mu_{g,1}/2$ and $\mu_2 \to \mu_{g,2}/2$, so Eq. (14) changes to:

$$F = \frac{\pi L c_i D_i}{2 \ln(\phi_2 / \phi_1)} \ln(p_1 / p_2) \tag{16}$$

The total oxygen flux can be expressed by:

$$F = J_{O_2} \times S \tag{17}$$

where J_{O_2} is the oxygen permeation flux measured in the experiment and S is the effective area of the membrane tube. If the oxygen transport is limited by the surface exchange at the interfaces, Eq. (15) gives:

$$J_{O_2} = \frac{\pi\phi_1\phi_2 LC_i k_{io}}{S(\phi_1+\phi_2)}\left(\sqrt{P_1/P_0} - \sqrt{P_2/P_0}\right) \quad (18)$$

where P_1 is the oxygen partial pressure on the shell side and P_2 is the oxygen partial pressure on the tube side. Eq. (18) predicts that the oxygen permeation flux (J_{O_2}, mol/cm^2.s) should be linearly proportional to the pressure term $(P_1/P_0)^{0.5}$-$(P_2/P_0)^{0.5}$ if only the surface exchange is the limiting step of the oxygen transport.

On the other hand, if the oxygen transport is only limited by the bulk diffusion through the membrane, the oxygen permeation flux is given by following formula:

$$J_{O_2} = \frac{\pi LC_i D_i}{2S\ln(\phi_{21}/\phi_1)}\ln(P_1/P_2) \quad (19)$$

Now the oxygen permeation flux, J_{O_2}, is linearly proportional to $\ln(P_1/P_2)$ if the limiting step is the bulk diffusion.

Figs. 4 and 5 plot the oxygen permeation flux against the oxygen partial pressure terms according to Eqs. (18) and (19), respectively. Fig. 4 shows that there is no linear relationship between the oxygen permeation flux and $(P_1/P_0)^{0.5}$-$(P_2/P_0)^{0.5}$ at the temperature ranges of 700 ^{o}C to 900 ^{o}C. However, a linear relationship of the oxygen permeation flux and $\ln(P_1/P_2)$ was found in Fig. 5 at the same temperature ranges. These phenomena demonstrate that the oxygen transport is limited by the bulk diffusion at the temperature ranges of 700 ^{o}C to 900 ^{o}C.

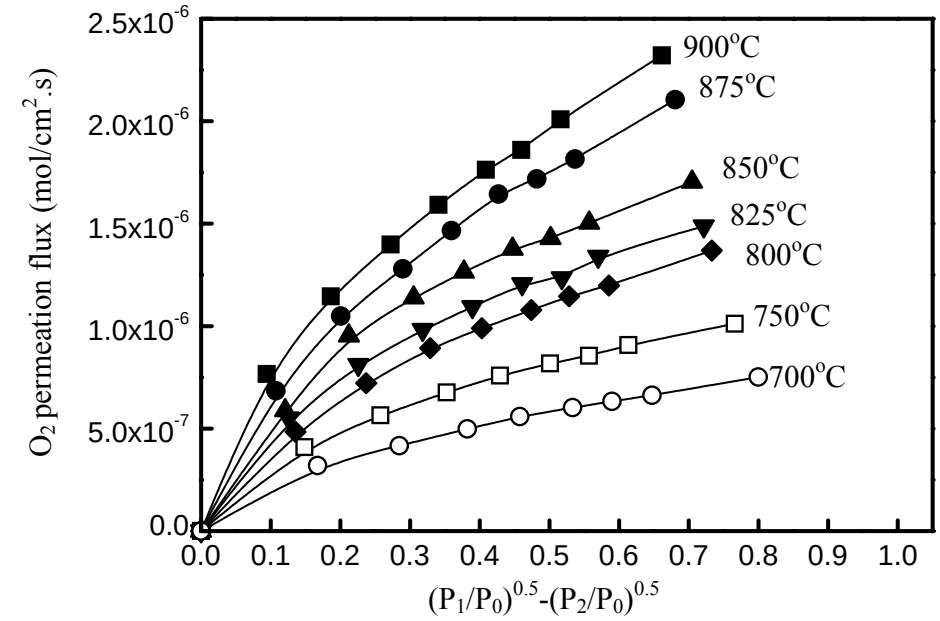

Fig. 4 Oxygen permeation flux through the BSCF membrane tube against $(P_1/P_0)^{0.5}$-$(P_2/P_0)^{0.5}$ at different temperatures.

Flow rates: a mixture of O_2 and N_2 = 300 ml/min, He = 60 ml/min, P_1 varied from 0.09 atm to 1 atm; P_2 varied from 0.0093 atm to 0.1147 atm. $Ø_2$=7.96 mm, $Ø_1$=4.56 mm, L=17.68 mm, S=2.531 cm^2.

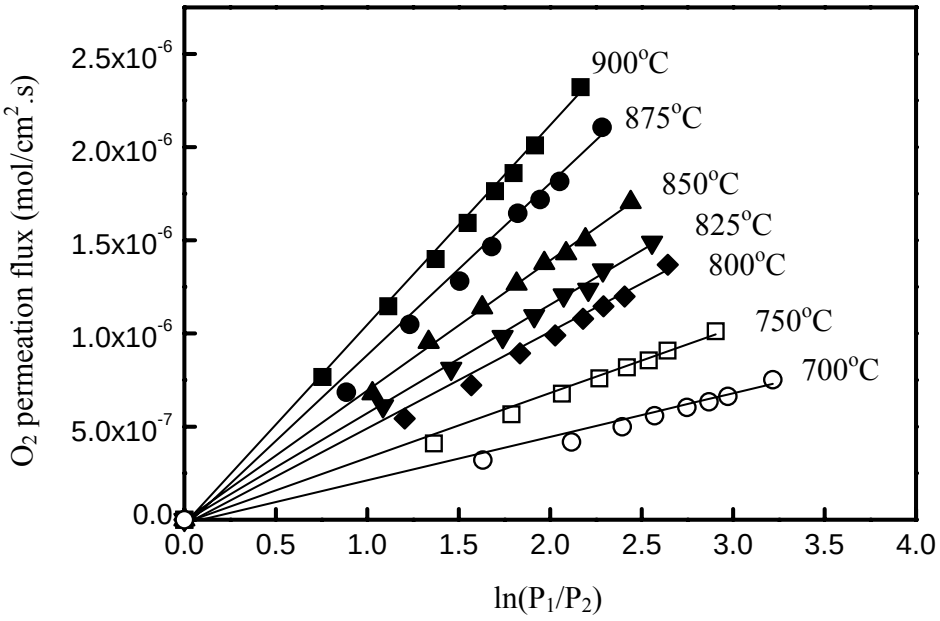

Fig. 5 Oxygen permeation flux through the BSCF membrane tube against ln (P_1/P_2) at different temperatures.

Flow rates: a mixture of O_2 and N_2 = 300 ml/min, He = 60 ml/min, P_1 varied from 0.09 atm to 1 atm; P_2 varied from 0.0093 atm to 0.1147 atm. $Ø_2$=7.96 mm, $Ø_1$=4.56 mm, L=17.68 mm, S=2.531 cm^2.

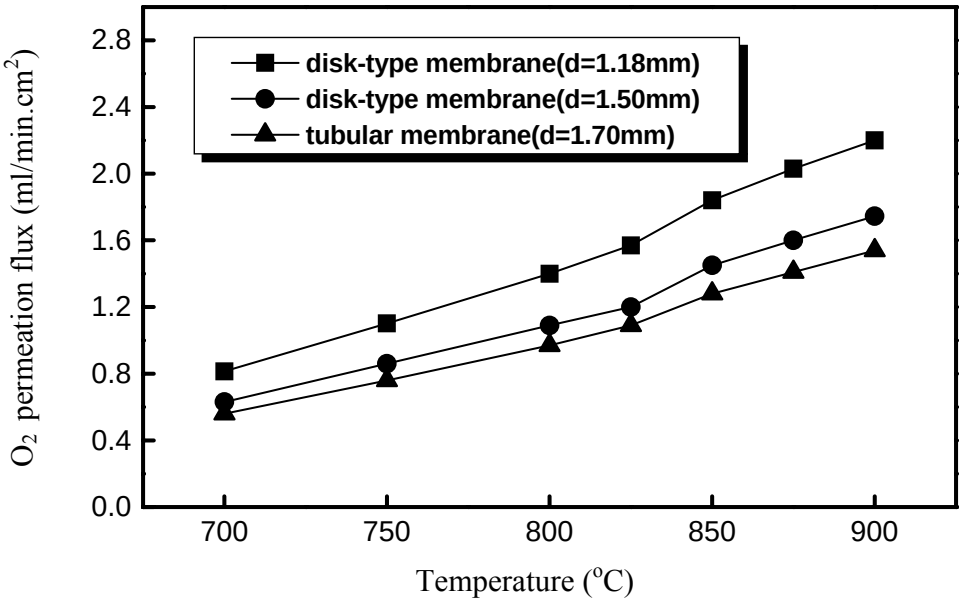

Fig. 6 Temperature dependence of the oxygen permeation flux of BSCF membranes of different thicknesses.

We also carried out the experiment about the thickness dependence of the oxygen permeation flux based on the BSCF disk-type membrane, as shown in Fig. 6. Under the same driving force, the oxygen permeation flux (J_{O_2}) through the membranes with different thicknesses (d) should follow Eq. (20) if the oxygen permeation is completely controlled by the bulk diffusion. Otherwise, it ought to follow Eq. (21) if the oxygen permeation is completely controlled by the surface exchange.

$$\frac{J_{O_2}(d_1)}{J_{O_2}(d_2)} = \frac{d_2}{d_1} \qquad (20) \qquad\qquad \frac{J_{O_2}(d_1)}{J_{O_2}(d_2)} = const. \qquad (21)$$

As shown in Fig. 6, the oxygen permeation flux through the membrane with different thicknesses almost fit Eq. (21). This result indicated that the oxygen permeation was mainly controlled by the bulk diffusion.

Based on the slopes of the lines in Fig. 5, we can calculate D_i at the indicated temperatures. The results are shown in Table 1. $D_v = D_i \times \frac{3-\delta}{\delta}$ was used to convert the measured D_i value to the oxygen vacancy diffusion coefficient, D_v [22]. Therefore, the oxygen vacancy diffusion coefficients D_v can be calculated from the D_i and the oxygen content at the different temperatures, the results are also shown in Table 1. S. Kim et al.

Table 1 Oxygen ion diffusion coefficient, oxygen content and the oxygen vacancy diffusion coefficient at different temperatures.

Temperature (^{o}C)	D_i (m^2/s)	3- δ	D_v (m^2/s)
900	3.31×10^{-10}	2.684	2.82×10^{-9}
875	2.83×10^{-10}	2.698	2.53×10^{-9}
850	2.34×10^{-10}	2.704	2.14×10^{-9}
825	1.87×10^{-10}	2.711	1.75×10^{-9}
800	1.68×10^{-10}	2.718	1.62×10^{-9}
750	1.16×10^{-10}	2.730	1.17×10^{-9}
700	0.77×10^{-10}	2.742	0.82×10^{-9}

[21] determined the D_v of the $SrCo_{0.8}Fe_{0.2}O_{3-\delta}$ (SCF) based on the model. The result was in a good agreement with those derived from the isotope exchange measurement. It was found that the corresponding D_v for the SCF ($D_v = 1.7\times10^{-9}$ m^2/s, at 890 ^{o}C) is higher than that for $La_{1-x}Sr_xCoO_{3-\delta}$ (x = 0, $D_v = 3.2\times10^{-10}$ m^2/s at 900 ^{o}C). The higher D_v was attributed to the reduction of the repulsive interaction generated from the oxygen vacancy migrating through the saddle point configuration (the triangle defined by two A cations and one B cation) because of the substitution of the smaller La^{3+} ion (r = 1.50 Å) in A-site by a larger Sr^{2+} ion (r = 1.58 Å). As expected, we also found that the D_v (D_v =

2.82×10^{-9} m^2/s, at 900 ^oC) for the BSCF is higher than that for the SCF ($D_v = 1.7\times10^{-9}$ m^2/s, at 890 ^oC). The reason is that the substitution of the smaller Sr^{2+} ion (r = 1.58 Å) in the SCF by the larger Ba^{2+} ion (r = 1.75 Å) results in the reduction of the repulsive interaction and the increase in the mobility of the oxygen vacancy.

4. Conclusion

The oxygen permeation flux through the BSCF perovskite membrane tube was determined at different oxygen partial pressures on the shell side and temperatures between 700 ^oC and 900 ^oC. The permeation rate of the BSCF perovskite membrane was found to be controlled by the bulk diffusion between 700 ^oC and 900 ^oC based on the dependence of oxygen permeation on the oxygen partial pressure. This result is in agreement with that from the thickness dependence of the oxygen permeation flux. The oxygen vacancy diffusion coefficients (D_v) of the BSCF perovskite membrane at different temperatures were calculated from the dependence of the oxygen permeation flux on the oxygen partial pressure based on the surface exchange fluxes model.

Acknowledgement

H. Wang greatly thanks the Alexander von Humboldt Foundation for the financial support.

References

[1] T. He, Q. Huang, A. P. Ramirez, Y. Wang, K. A. Regan, N. Rogado, M. A. Hayward, M. K. Haas, J. S. Slusky, K. Inumara, H. W. Zandbergen, N. P. Ong, R. J. Cava, Nature 54 (2001) 411.

[2] Y. Xu, C. McCammon, B.T. Poe, Science 282 (1998) 922.

[3] D. D. Fong, G. B. Stephenson, S. K. Streiffer, J.A. Eastman, O. Auciello, P. H. Fuoss, C. Thompson, Science 304 (2004) 1650.

[4] J. Junquera, P. Ghosez, Nature 422 (2003) 506.

[5] C. C. Homes, T. Vogt, S. M. Shapire, S. Wakimoto, A. P. Ramirez, Science 293 (2001) 673.

[6] Y. Moritomo, A. Asamitsu, H. Kuwahara, Y. Tokura, Nature 380 (1996) 141.

[7] Y. Teraoka, T. Nobunaga, N. Yamazoe, Chem. Lett. 195 (1988) 503.

[8] H. H. Wang, Y. Cong, W. S. Yang, J. Membr. Sci. 210 (2002) 259.

[9] U. Balachandran, J. T. Dusek, P. S. Maiya, B. Ma, R. L. Mieville, M. S. Kleefish, C. A. Udovich, Catal. Today 36 (1997) 117.

[10] H. H. Wang, Y. Cong, W. S. Yang, Catal. Today 82 (2003) 157.

[11] C. Y. Tsai, A. G. Dixon, W. R. Moser, Y. H. Ma, AIChE J. 43 (1997) 2741.

[12] H. H. Wang, Y. Cong, W. S. Yang, Chinese Science Bulletin 47 (7) (2002) 534.

[13] S. Xu, W. J. Thomson, AIChE J. 43 (1997) 2731.

[14] H. H. Wang, Y. Cong, W. S. Yang, Chem. Comm 14 (2002) 1468.

[15] F. T. Akin, Y. S. Lin, J. Membr. Sci. 209 (2002) 457.

[16] H. H. Wang, Y. Cong, W. S. Yang, Catal. Lett. 84 (2002) 101.

[17] H. H. Wang, Y. Cong, X. F. Zhu, W. S. Yang, React. Kinet. Catal. Lett. 79 (2003) 351.

[18] Z. P. Shao, W. S. Yang, Y. Cong, H. Dong, J. H. Tong, G. X. Xiong, J. Membr. Sci. 172 (2000) 177.

[19] H. H. Wang, Y. Cong, W. S. Yang, 209 (2002) 143.

[20] S. Kim, Y. L. Yang, R. Christoffersen, A. J. Jacobson, Solid State Ionics. 109 (1998) 187.

[21] S. Kim, Y. L. Yang, A. J. Jacobson, B. Abeles, Solid State Ionics. 106 (1998) 189.

[22] A. Thursfield, I. S. Mercalfe, J. Mater. Chem., 14 (2004) 2475.